

# Experimental validation of the theoretical prediction for the optical $S$ matrix

A. M. Martínez-Argüello,<sup>1</sup> V. Domínguez-Rocha,<sup>1</sup> R. A. Méndez-Sánchez,<sup>1</sup> and M. Martínez-Mares<sup>2</sup>

<sup>1</sup>*Instituto de Ciencias Físicas, Universidad Nacional Autónoma de México,  
Apartado Postal 48-3, 62210 Cuernavaca, Mor., Mexico*

<sup>2</sup>*Departamento de Física, Universidad Autónoma Metropolitana-Iztapalapa,  
Apartado Postal 55-534, 09340 Ciudad de México, Mexico*

Scattering of waves is omnipresent in nature in systems with sizes varying from  $10^{-15}$  to  $10^{25}$  m. Within this 40 orders of magnitude, in a great number of systems, the scattering can be separated in an averaged response that crosses rapidly the scattering region and a fluctuating delayed response. This fact is the basis of the optical model; the averaged response, represented by the optical matrix  $\langle S \rangle$ , is composed with the fluctuating part that can be taken as a random matrix. Although the optical model was developed more than 60 years ago, a theoretical prediction for the optical matrix was obtained until very recently. The validity of such prediction is experimentally demonstrated here. This is done studying the scattering of torsional waves in a quasi-1D elastic system in which a locally periodic system is built; the distribution of the scattering matrix is calculated completely free of parameters. In contradistinction to all previous works, in microwaves and in elasticity, in which the value of  $\langle S \rangle$  is obtained from the experiment, here the theoretical prediction is used to compare with the experiment. Numerical simulations show that the theoretical value is still valid when strong disorder is present. Several applications of the theoretical expression for the optical matrix in other areas of physics are proposed. Possible extensions of this work are also discussed.

PACS numbers: 72.10.-d, 73.63.-b, 73.23.-b

The scattering amplitudes, in almost all physical wave systems, can be separated in a component passing rapidly through the scattering region plus a delayed response coming from multiple scattering. This fact is summarized in the optical model in which the dispersion amplitudes are separated into an averaged part and a fluctuating part. The averaged response is captured by the optical matrix  $\langle S \rangle$  while the fluctuations are commonly studied using statistical techniques from random matrix theory. Therefore, the optical matrix has become a fundamental quantity in the description of multiple scattering of particles and waves. It was introduced in the optical model of the nucleus developed in the 1950's by Feshbach, Porter and Weisskopf [1, 2]. Since the scattering of a nucleon by an atomic nucleus is equivalent to the theory of waveguides [3], this model has been extended not only to chemical reactions but also to electronic transport through ballistic quantum dots and microwave cavities [4, 5] and more recently to mechanical waves [6, 7].

The average  $\langle S \rangle$  can be physically interpreted as the fraction of the incident wave packet which comes out promptly from the scattering region [1]. A concrete realization of  $\langle S \rangle$  was proposed in Ref. [8] in the transport of electrons in mesoscopic systems: when the incoming and outgoing channels are not coupled perfectly to the internal system, the optical matrix  $\langle S \rangle$  quantifies the coupling between the internal and external regions. This is very important since the imperfect coupling has to be taken into account in almost all scattering experiments [6, 9–15]. Furthermore, as a consequence of the analyticity of the  $S$  matrix, even when absorption is present [16, 17], wave scattering systems are self-averaging [5]. This means that  $\langle S \rangle$  is the only relevant

parameter needed to obtain all scattering properties in complex systems since the fluctuations seem to be universal depending only on very general symmetry properties as presence/absence of time reversal invariance, among others.

There are, on the one hand, several theoretical studies in which  $\langle S \rangle$  is used to obtain the distribution of the scattering matrix known as Poisson's kernel [18–21]. In the one channel case it reads

$$p_{\langle S \rangle}(S) = \frac{1}{2\pi} \frac{1 - |\langle S \rangle|^2}{|S - \langle S \rangle|^2}, \quad (1)$$

where  $S = e^{i\theta}$ . An analytical value for  $\langle S \rangle$  was missing during more than 60 years; it was obtained only very recently for a one-dimensional chain of delta potentials [22]. On the other hand, up to now, there are no experimental studies about  $\langle S \rangle$ . In all experiments performed in microwave cavities and graphs, and in elastic systems, the value of  $\langle S \rangle$  is obtained afterwards from the measurement since an analytical expression for it was not available at that time. Then, to compare with the experiment, the numerical value obtained from the experiment is used in the theoretical expression of Poisson's kernel in a kind of self-consistent argument.

Since the experiment is the only mechanism to validate a theoretical development, in this paper, using elastic waves, we experimentally demonstrate the validity of the theoretical prediction for the optical matrix  $\langle S \rangle$  given in Ref. [22]. To do this the scattering of torsional waves in a beam, in which a finite crystalline structure is machined, is studied. In contradistinction with the methods of Refs. [23, 24], here, to obtain the optical matrix in this system, the scattering formalism developed in

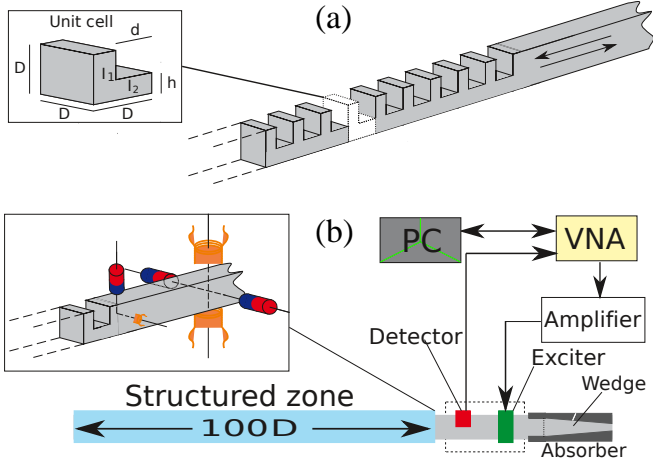


FIG. 1. (a) Aluminum beam ( $\sqrt{G/\rho} = 3104.7$  m/s) which consists of a region with a locally periodic structure, composed of  $N$  scatterers, and a semi-infinite uniform region of squared cross-section. The unit cell (inset) of length  $D$  consists of bodies 1 and 2 of lengths  $D - d$  and  $d$ , with polar moments of inertia  $I_1$  and  $I_2$ , respectively. We use  $w_1 = h_1 = w_2 = D = 2.54$  cm,  $h_2 = h = 0.9525$  cm and  $d = 1.5875$  cm. (b) Setup: a beam consists of a structured zone, a wedge zone with an absorber, and a free region where the exciter and detector are located. Inset: The coils of the EMAT are connected in series and their polarity is such that the EMAT excites only torsional waves. The EMAT detector is composed of a magnet and a small coil.

Ref. [25] is applied to the elastic crystalline structure. As we will see below the distribution of the scattering matrix, with the theoretical value of  $\langle S \rangle$ , correctly predicts the results measured with acoustic resonant spectroscopy completely free of parameters. Numerical results when disorder is present, are also given.

Lets consider the semi-infinite beam of Fig. 1 (a) in which a locally periodic structure of  $N$  notches is machined, such that the unit cell is formed by two parts or bodies labeled as 1 and 2. Plane waves are sent to the structure from the uniform part and the response of the system is obtained using the scattering matrix formalism. The stationary solution  $\psi_j(x)$  of the one-dimensional wave equation describing torsions, in the  $j$ th body of the unit cell of Fig. 1, is a superposition of waves traveling to the left and to the right  $\psi_j(x) = a_j e^{-ik_j x} + b_j e^{ik_j x}$ , where  $j(=1, 2)$  indicates the corresponding part of the unit cell and  $k_j$  is the wave number related to the frequency by  $k_j = 2\pi f/c_j$  with  $c_j = \sqrt{G\alpha_j/\rho I_j}$  the phase velocity of the torsional waves. Here,  $\rho$  is the density of the rod,  $G$  its shear modulus,  $I_j$  the polar moment of inertia of part  $j$ , and  $\alpha_j$  the Navier series,

$$\alpha_j = \sum_{m=0}^{\infty} \sum_{p=0}^{\infty} \frac{256/\pi^6}{(2m+1)^2(2p+1)^2} \frac{h_j w_j}{\left(\frac{2m+1}{h_j}\right)^2 + \left(\frac{2p+1}{w_j}\right)^2}, \quad (2)$$

with  $w_j$  and  $h_j$  the width and height of body  $j$ .

The boundary conditions between bodies 1 and 2, which are in contact at a point  $x = x'$ , are continuity of the wave amplitude,  $\psi_1(x') = \psi_2(x')$ , and continuity of the moment of torsion,  $M_{T_1}(x') = M_{T_2}(x')$ . The latter is related to the derivative of the wave amplitude through  $M_{T_j}(x) = G\alpha_j \partial \psi_j(x) / \partial x$ . Thus, the derivative of the wave amplitude, at the point  $x = x'$ , is discontinuous by a factor  $\eta = \alpha_2/\alpha_1$  when the same material is used in bodies 1 and 2. Since the two parts of the unit cell oscillate with the same frequency, the wave numbers of both bodies are related through  $k_1 = k_2 c_2/c_1 = k_2 \sqrt{\eta I_1/I_2}$ , where  $I_1 = \frac{1}{6}D^4$  and  $I_2 = \frac{1}{6}D^4 \left(2\frac{h}{D} - 3\frac{h^2}{D^2} + 2\frac{h^3}{D^3}\right)$  are the polar moments of inertia of bodies 1 and 2, of the unit cell of length  $D$ , respectively. To calculate  $I_2$  the parallel axes theorem was used with a distance  $(D - h)/2$ .

The reflection and transmission amplitudes through a single scatterer are

$$r_n = \frac{2i\beta \sin(k_2 d)}{\beta^2 e^{ik_2 d} - e^{-ik_2 d}} \quad \text{and} \quad t_n = \frac{\beta^2 - 1}{\beta^2 e^{ik_2 d} - e^{-ik_2 d}}, \quad (3)$$

where  $\beta = (k_1 - \eta k_2)/(k_1 + \eta k_2)$  and  $d$  is the scatterer length. These were obtained using the boundary conditions at both sides of the notch, solving the resulting system of equations. The response of the system of  $N$  scatterers is described by the  $1 \times 1$  scattering matrix  $S_N$ , which is related to the scattering matrix  $S_{N-1}$ , that describes the system with  $N - 1$  scatterers, through the following recurrence relation [25]

$$S_N = (r_n z_n^* + z_n S_{N-1})(r_n^* z_n + z_n^* S_{N-1}^*)^{-1} S_{N-1}^* \quad (4)$$

where  $z_n = t_n e^{ik_1(D-d)}$ . The wave number  $k_1$  is the tunable parameter, proportional to the frequency, since the uniform part of the beam has the same transversal area as body 1 of the unit cell. According to Refs. [22, 25–27], the recurrence relation given in Eq. (4) can be interpreted as a non-linear map, for the phase of the scattering matrix, that reveals the forbidden and allowed bands as a function of  $k_1$  (see upper panel of Fig. 2). This non-linear mapping accepts stable and unstable fixed point solutions when  $N \rightarrow \infty$ , the latter being a set of zero measure that will be ignored. A fixed point solution can be interpreted as the optical matrix,  $\langle S \rangle$ , since it satisfies the analyticity condition  $\langle S^N \rangle = \langle S \rangle^N$  [22]. The values of the optical matrix in an allowed band is (we are interested in this region only)

$$\langle S \rangle = i(r_n^* z_n)^{-1} \left[ -\sqrt{|t_n|^4 - (\text{Re } z_n)^2} + \text{Im } z_n \right]. \quad (5)$$

It is remarkable that the optical matrix  $\langle S \rangle$ , and Poisson's kernel, Eq. (1), is completely determined (and only depends) on the values of the reflection and transmission amplitudes of a single scatterer, no matter how they are obtained, by numerical or experimental methods or by a theoretical model as in Eq. (3).

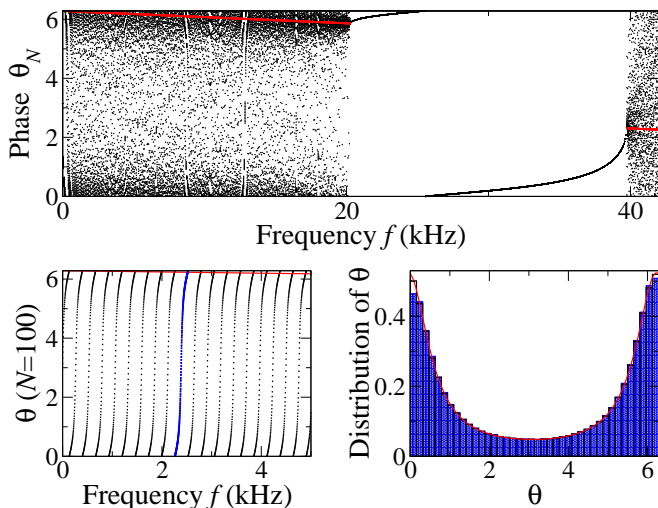


FIG. 2. (Color online) Upper panel: the last 15 iterations, of 1000, of Eq. (4), are plotted as a function of the frequency with an initial condition  $\theta_0 = \pi$ . The red line corresponds to the phase of  $\langle S \rangle$  in Eq. (5). Lower panels: in the left panel the resonances of the phase of Eq. (4), for  $N = 100$ , are shown. The histogram of the resonance highlighted in blue is shown in the right panel. More details of the right panel are given in the text.

In the upper panel of Fig. 2 the band structure in frequency is observed for the last 15 iterations of 1000. The allowed bands are clearly observed (the first band and a part of the second one are shown) since the iterations cover the full interval between 0 and  $2\pi$  for the phase in a non uniform way. It can be also observed in the forbidden bands, only one is shown, that the iterations reach a single fixed point. The solution in the allowed bands, given by Eq. (5), is also plotted. This solution corresponds to the maximum of the distribution around which  $\theta_N$  is distributed. In the left lower panel of Fig. 2 the phase  $\theta_N$ , for  $N = 100$ , shows the resonances as a function of the frequency in an allowed band; resonances do not appear in the forbidden band. As it can be seen in this figure, the phase do not increase linearly; the largest slope is associated to the resonant peaks. The distribution of the phase in the first allowed band is studied numerically in two different ways. Firstly, the distribution of the phase for  $10^4$  realizations (iterations) for the fixed frequency  $f = 2395$  Hz, is plotted in the right lower panel of Fig. 2 as a black histogram. Secondly, the (blue) bars in the same figure represent the histogram of the phase along the resonance centered at  $f = 2395$  Hz; the maximum of the distribution corresponds to the lowest slope of the phase given in the left lower panel of the same figure. This resonance is (blue) highlighted in the left lower panel. Also, in the same figure, the distribution of the Poisson kernel, given by Eq. (1) with the average of the scattering matrix  $\langle S \rangle$  of Eq. (5) for  $f = 2395$  Hz, is plotted (continuous red curve). An excellent agree-

ment between the numerical histograms and the theoretical distribution is obtained. This result is relevant for experimental implementation since it allows to study a specific resonance of a given sample, instead of several sample realizations.

In what follows we will show that Poisson's kernel, with the average taken from Eq. (5), correctly predicts the experimental distribution of the scattering matrix in elastic waves. This will be done for a system with a large, but fixed, number of scatterers within a small frequency range in the first allowed band. The experimental setup is shown in Fig. 1 (b). A signal of frequency  $f$ , produced by a vector network analyzer (VNA, Anritsu MS-4630B) and intensified by a Cerwin-Vega (CV-900) high-fidelity audio amplifier, is sent to an electromagnetic acoustic transducer (EMAT) designed *ad hoc* for this experiment since high power and selectivity is needed. This transducer, composed by two coils and two permanent magnets, shown in the inset, produces torsional vibrations that propagate through the system [28, 29]. The response, measured by another EMAT, is directly sent to the VNA. The measurements, amplitude and phase, as a function of the frequency  $f$ , are taken from the VNA to the computer through a GPIB port.

The system under study consists of an aluminum beam of squared cross-section of width  $D = 2.54$  cm and length 3.6 m divided in three regions. From a free boundary, a locally periodic structure, composed of 100 equal notches as in Fig. 1 (b), is machined. The middle part of the beam, of 56 cm length, remains uniform. In this part the waves are excited and the scattering matrix is measured. The other end simulates a semi-infinite beam by means of a passive vibration isolation (PVI) system that absorbs the incoming waves [6, 7, 30, 31]. The PVI system, is composed of a wedge and polymeric foams and has length of 50 cm, covering completely the wedge and part of the uniform section of the beam. This system allows the measurement of the mechanical scattering matrix, in the frequency domain, since the normal modes of the complete beam cannot be established.

In Fig. 3 (left panels) the measured amplitude and phase of the scattering matrix, as a function of the frequency, for a part of the first band, is shown. As expected, several resonances of the allowed band, for which the phase takes values between 0 and  $2\pi$ , are observed. All of these resonances describe, in the Argand plane, non-concentric circles of different radii. This is due to the impedance of the detector [6, 7]. We analyze the phase of the resonance lying between the dotted lines, from 2530.0 to 2638.8 Hz, using the method of Ref. [6] to subtract the shift due to the impedance. As seen in the right upper panel of the same figure, this corrected  $S$  matrix describes a circle centered at the origin (the radius was set to 1 for convenience). The distribution of the phase along the circle is shown in the lower panel as a histogram. In the same figure the analytical distribution expressed by

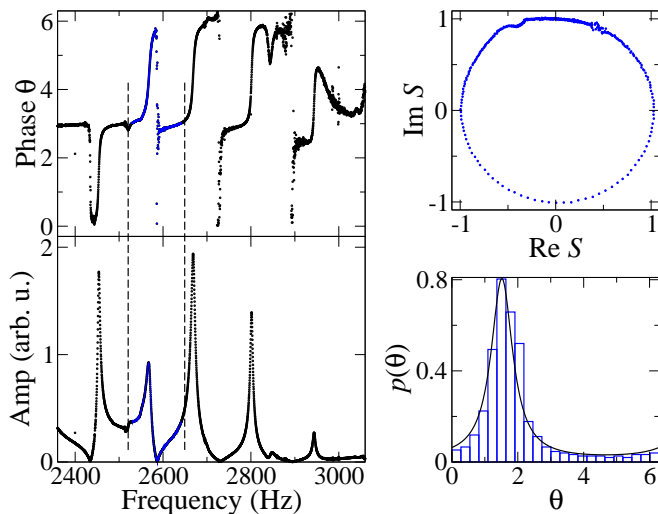


FIG. 3. (Color online) Amplitude and phase of the  $S$ -matrix as a function of the frequency (left panels). Shifted and normalized  $S$ -matrix in the Argand plane (upper right panel), in a part of the allowed band. The histogram of the highlighted resonance (blue) at  $f = 2570$  Hz and its comparison to the Poisson kernel, Eq. (1) with  $\langle S \rangle$  given by Eq. (5), is shown in the right lower panel. The dimensions of the unit cell are the same as in Fig. 1 but  $h$  replaced by an effective value,  $0.746h$ , due to the punching of body 2 [28].

the Poisson kernel, Eq. (1), continuous line, is also given. The value of the optical matrix was taken from Eq. (5) evaluated at  $f = 2570$  Hz, the center of the resonance. A very good agreement between theory and experiment is observed. The only effective parameter used is the one related to the punching of body 2 by body 1. This parameter appears because of the one-dimensional character of the  $S$ -matrix theory used whereas the constructed beam, given in Fig. 1 (a), is three-dimensional.

Now the robustness of the expression of the optical matrix, with respect to disorder, losses and noise will be addressed. The effect of the disorder in Eq. (5) is studied numerically varying randomly the depth of the groove with a uniform distribution of width  $\delta$ . That is, the height  $h_2$  of body 2 is varied according to  $h_2 =$

$h + \epsilon(D - h)$ , where  $\epsilon$  is uniformly distributed in the interval  $[0, \delta]$ . Thus  $\delta$  quantifies the disorder strength and  $\delta = 0$  corresponds to the crystalline structure. In Fig. 4 the last 15 iterations of 1000 are plotted for different values of the disorder between 10% and 90%. As it can be seen there, the band structure is preserved for low values of the disorder strength whereas for high disorder the band structure disappears. The prediction of the optical matrix agree with the maximum of the distribution for values of the wavenumber in the middle of the first band whereas in the gap and in the second band high deviations are visible. The resulting distributions, for different values of the disorder strength, are shown also in Fig. 4. The distributions of the phase agree with Poisson's kernel, even for very high values of the disorder strength. This result is relevant since it shows the universality of the fluctuations against disorder. The used  $\langle S \rangle$  was obtained averaging the values of  $r_n$  and  $t_n$  from the disorder. Some results about the effect of the losses in the optical matrix prediction can be obtained directly from the experiment since absorption is always present. Contrary to the case in chaotic systems [11, 32], in which a generalization of Poisson's kernel appears, in the beam worked here the absorption only gives a shift that can be taken into account in the normalization as in Refs. [6, 7, 17]. In Fig. 5(a) the measured amplitude, within the first pass-band, as a function of the frequency, is given. As it can be seen in panels (f) and (g) of the same figure, regardless of the location of the resonance within the allowed band, the agreement between Poisson's kernel, Eq. (1), and the experimental results is excellent. As it can be seen roughly in panel (a) of this figure, as frequency increases the signal becomes smaller. This is evidenced in panels (b), (c), (d) and (e), in which the measured  $S$  is plotted for the resonances highlighted in panel (a), with the same order. On approaching the forbidden band the signal becomes weak and noisy, panels (d) and (e). Then  $S$  does not lie in a circle anymore but it lies in a ring. This effect produces a diminishing of the optical matrix,  $\langle S \rangle$ , that tend to flatten the distribution, panels (h) and (i), in a similar way that in the disordered case.

**Concluding remarks and outlook.** The good agreement observed between the theory and the experiment represents the validation of the analytical expression of the optical matrix  $\langle S \rangle$  through the invariant density of the phase of the  $S$ -matrix, the Poisson kernel, that results from a non trivial relation between coherent transport and deterministic maps [27]. The detected torsional waves outside the locally periodic system, a square cross-section beam with 100 notches, correspond to the  $1 \times 1$  scattering matrix  $S$  once they are excited also outside. The measured distribution of the phase of  $S$  of a single

resonance agrees with Poisson's kernel using the theoretical prediction given in Eq. (5); the optical matrix given in that equation depends only on (i) the  $S$ -matrix composition rule and (ii) the reflection and transmission coefficients of a single unit cell. Thus the prediction for the optical matrix is quite general, with details depending on the constituents of the particular system, and Eq. (5) can be applied to a plethora of wave systems of different nature just having the reflection and transmission of a single scatterer. Several applications are expected in different areas since there are many realizations of a

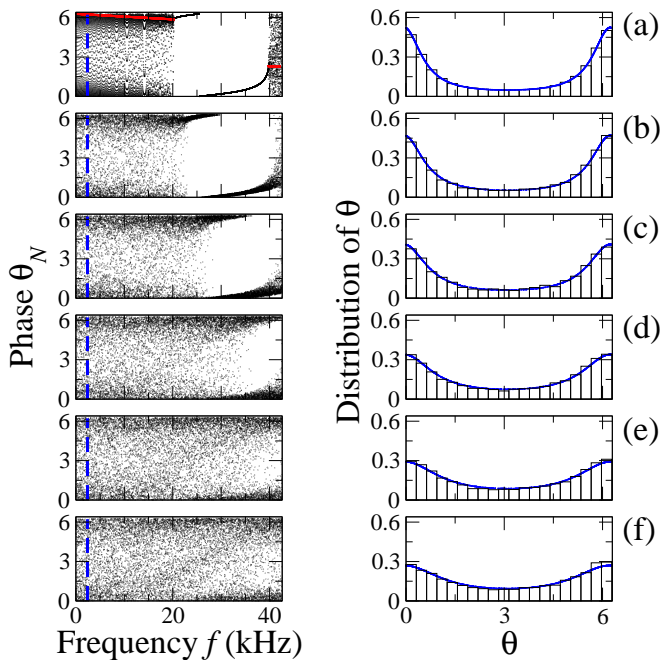


FIG. 4. (Color online) Left: the last 15 iterations, of 1000, of Eq. (4), are plotted as a function of the frequency with an initial condition  $\theta_0 = \pi$  for different degrees of disorder: (a) 0%, (b) 10%, (c) 25%, (d) 50%, (e) 75% y (f) 90%. The red line corresponds to the phase of  $\langle S \rangle$  in Eq. (5); it is valid for all panels at the left since only indistinguishable changes appear. The respective histograms of the phase are given in the right panels. The continuous curve is the Poisson kernel, Eq. (1), with  $\langle S \rangle$  given by Eq. (5) averaged over the disorder realizations.

semi-infinite one-dimensional periodic system composed by two media, *i.e.* a photonic crystal, a superlattice, a layered media in geology, etc. In fact data of the microwave ring, used to measure the Hofstadter’s butterfly and transmission through a locally periodic are available [11, 24]. The results are also valid for compressional waves [28]. Applications in the terahertz [33] and in the optical [34–36] regimes seem also possible since frequency duplicators/dividers can be used to measure the phase. Another system in which the formalism can be applied is a 1D tight-binding chain [37]. This model is ubiquitous in condensed matter [38], material science and chemistry and has several applications since the transmission and reflection coefficients can also be obtained [39]. In fact this model has realizations in chains of dielectric scatterers [40, 41], in the evolution of excitations in molecular chains and in molecular rings (using nuclear magnetic resonance) [42, 43]. Microwave billiards [9–11, 44] and graphs [12] are also well suited to perform different tests since the applicability of the equation to cells with more complex scatterers, as in a chain of cavities [45, 46] is also possible. These kind of chains have been constructed with microwave billiards [47] and can also be constructed with thin plates [30, 48]. The Heidelberg

approach [49], a methodology in which the scattering matrix is built in terms of a Hamiltonian and the couplings to the exterior, is optimal for applications of Eq. (5). In fact, results of the prompt response could be possible for nuclear systems, in particular for neutron scattering, which only see the nuclei but not the electrons, would see –and identify– the periodic structure. Elastic scattering is part of nuclear reactions, and lots of data are available for (differential) cross sections and scattering of protons, electrons, or neutrons of individual nuclei. Although phase shifts are not observables, unlike cross sections, it is possible to get non univocal phase shifts from cross sections having a model (potential). Apart of other effects (as absorption, decoherence, PT-symmetric, more dimensions or a higher number of channels) that have to be included, there are many applications that could be worked out. A simple example can be thought in astrophysics: Although in supercooled neutron stars the more recent models are in favour of degenerate baryon models forming stellar superfluids [50], within the BardeenCooperSchrieffer theory, there are other models that consider crystallization in one dimension and pairing in the perpendicular planes [51].

This work was supported by DGAPA-UNAM (grant IN109318) and by CONACyT (grant CB-2016/285776). VDR and AMMA were supported by DGAPA. We thank G. Báez, A. Méndez-Bermúdez, T. H. Seligman, H. Pastawski, T. Papenbrook, and D. Page for useful comments and to “Centro Internacional de Ciencias A. C.” for several meetings held there and the given facilities for the laboratory.

- 
- [1] H. Feshbach, *Topics in the theory of nuclear reactions*, in *Reaction dynamics*, edited by E. W. Montroll, G. H. Vineyard, M. Levy, and P. T. Matthews (Gordon and Breach, New York, 1973) p. 169.
  - [2] H. Feshbach, C. E. Porter, and V. F. Weisskopf, *Phys. Rev.* **96**, 448 (1954).
  - [3] T. Ericson and T. Mayer-Kuckuk, *Ann. Rev. Nuclear Sci.* **16**, 183 (1966).
  - [4] P. A. Mello and H. U. Baranger, *Waves Random Media* **9**, 105 (1999).
  - [5] P. A. Mello and N. Kumar, *Quantum Transport in Mesoscopic Systems: Complexity and Statistical Fluctuations* (Oxford University Press, New York, 2005).
  - [6] G. Báez, M. Cobián-Suárez, A. M. Martínez-Argüello, M. Martínez-Mares, and R. A. Méndez-Sánchez, *Acta Phys. Pol. A*, **124**, 1069 (2013).
  - [7] A. M. Martínez-Argüello, M. Martínez-Mares, M. Cobián-Suárez, G. Báez, and R. A. Méndez-Sánchez, *EPL* **110**, 54003 (2015).
  - [8] P. W. Brouwer and C. W. J. Beenakker, *Phys. Rev. B* **55**, 4695 (1997).
  - [9] R. A. Méndez-Sánchez, U. Kuhl, M. Barth, C. H. Lewenkopf, and H.-J. Stöckmann, *Phys. Rev. Lett.* **91**, 174102 (2003).

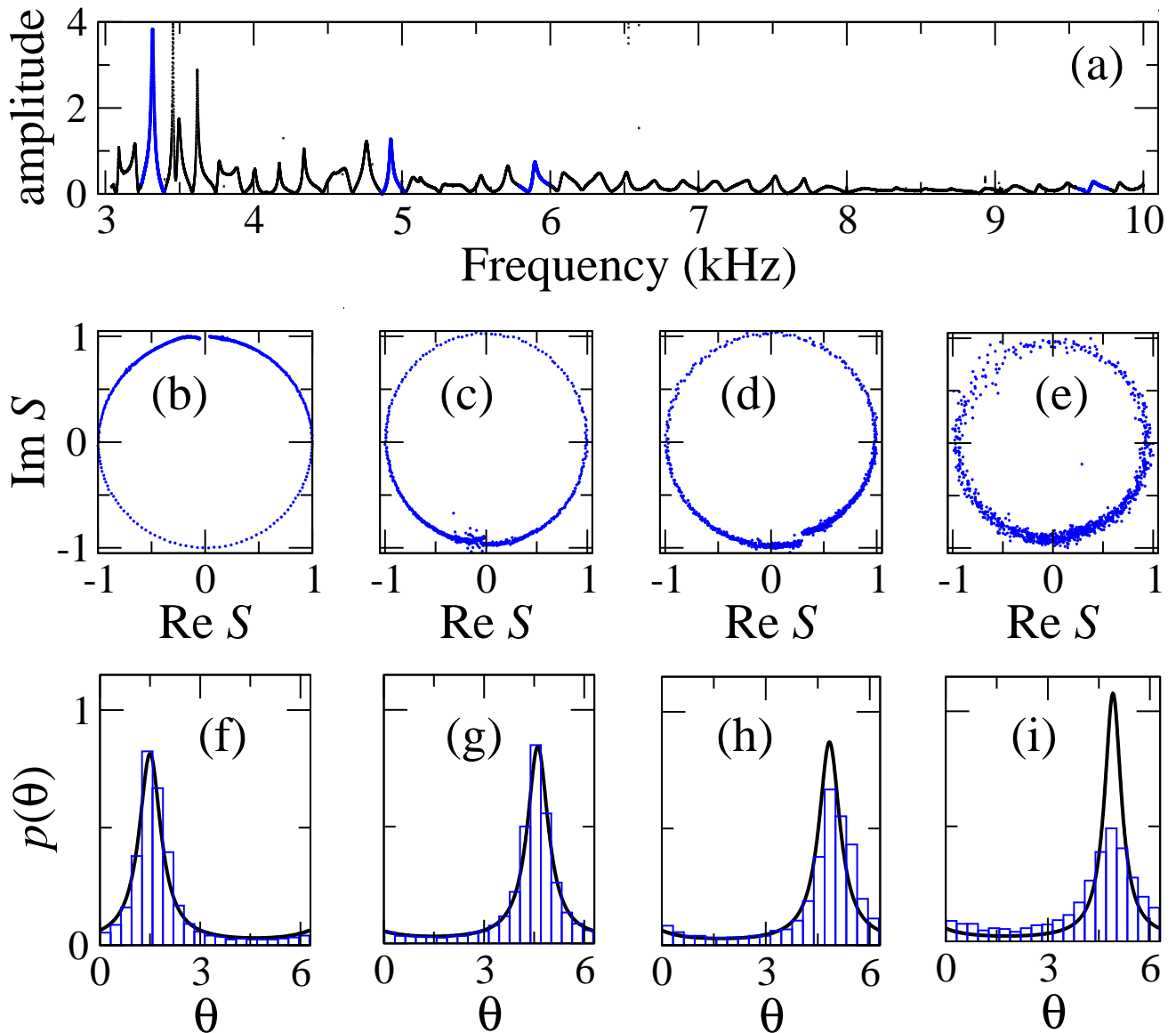


FIG. 5. (Color online) (a) measured amplitude (in arbitrary units) as a function of the frequency. The analyzed resonances (b), (c), (d) and (e), and their respective histograms (f), (g), (h), and (i), are taken in the intervals [3244.0, 3399.0] Hz, [4859.8, 5019.8] Hz, [5792.0, 5998.0] Hz, and [9560.0, 9760.0] Hz, respectively. The continuous line in the lower panels is the Poisson kernel, Eq. (1), with  $\langle S \rangle$  given by Eq. (5).

- [10] S. Hemmady, X. Zheng, E. Ott, T. M. Antonsen, and S. M. Anlage, *Phys. Rev. Lett.* **94**, 014102 (2005).
- [11] U. Kuhl, M. Martínez-Mares, R. A. Méndez-Sánchez, and H.-J. Stöckmann, *Phys. Rev. Lett.* **94**, 144101 (2005).
- [12] M. Lawniczak, S. Bauch, O. Hul, and L. Sirko, *Phys. Scr.* **T147**, 014018 (2012).
- [13] Y. Aurégan, V. Pagneux, *Acta Acustica united with Acustica* **102**, 869–875 (2016).
- [14] A. M. Martínez-Argüello, A. Rehemangiang, M. Martínez-Mares, J. A. Méndez-Bermúdez, H.-J. Stöckmann, and U. Kuhl, *Phys. Rev. B* **98**, 075311 (2018).
- [15] M. Lawniczak and L. Sirko *Sci. Rep.* **9**, 5630 (2019).
- [16] V. A. Gopar, M. Martínez-Mares, and R. A. Méndez-Sánchez, *J. Phys. A: Math. Theor.* **41**, 015103 (2008).
- [17] A. M. Martínez-Argüello, R. A. Méndez-Sánchez, and M. Martínez-Mares, *Phys. Rev. E* **86**, 016207 (2012).
- [18] G. López, P. A. Mello, and T. H. Seligman, *Z. Phys. A* **302**, 351 (1981).
- [19] P. A. Mello, P. Pereyra, and T. H. Seligman, *Ann. Phys. (N.Y.)* **161**, 254 (1985).
- [20] W. Friedman and P. A. Mello, *Ann. Phys. (N. Y.)* **161**, 276 (1985).
- [21] Y. Fyodorov and D. V. Savin, *Resonance Scattering of Waves in Chaotic Systems*, in *The Oxford Handbook of Random Matrix Theory*, edited by G. Akemann, J. Baik, and P. Di Francesco (Oxford University Press, Oxford, New York, 2011) Ch. 34.
- [22] V. Domínguez-Rocha, R. A. Méndez-Sánchez, M. Martínez-Mares, and A. Robledo, arXiv:1509.00814.

- [23] D. J. Griffiths and C. A. Steinke, *Am. J. Phys.* **69**, 137 (2001).
- [24] G. A. Luna-Acosta, H. Schanze, U. Kuhl, and H.-J. Stöckmann, *New J. Phys.* **10**, 043005 (2008).
- [25] V. Domínguez-Rocha and M. Martínez-Mares, *J. Phys. A: Math. Theor.* **46**, 235101 (2013).
- [26] M. Martínez-Mares and A. Robledo, *Phys. Rev. E* **80**, 045201(R) (2009).
- [27] M. Martínez-Mares, V. Domínguez-Rocha, and A. Robledo, *Eur. Phys. J. Special Topics* **226**, 417 (2017).
- [28] A. Morales, J. Flores, L. Gutiérrez, and R. A. Méndez-Sánchez, *J. Acoust. Soc. Am.* **112**, 1961 (2002).
- [29] J. A. Franco-Villafañe, E. Flores-Olmedo, G. Báez, O. Gandarilla-Carrillo, and R. A. Méndez-Sánchez, *Eur. J. Phys.* **33**, 1761 (2012).
- [30] E. Flores-Olmedo, A. M. Martínez-Argüello, M. Martínez-Mares, G. Báez, J. A. Franco-Villafañe, and R. A. Méndez-Sánchez, *Sci. Rep.* **6**, 25157 (2016).
- [31] A. Arreola-Lucas, G. Báez, F. Cervera, A. Climente, R. A. Méndez-Sánchez and J. Sánchez-Dehesa, *Sci. Rep.* **9**, 1860 (2019).
- [32] R. B. do Carmo and F. M. de Aguiar, *Sci. Rep.* **9**, 3634 (2019).
- [33] S. S. Dhillon *et al* *J. Phys. D: Appl. Phys.* **50**, 043001 (2017).
- [34] M. I. Tribelsky, S. Flach, A. E. Miroshnichenko, A. V. Gorbach, and Y. S. Kivshar, *Phys. Rev. Lett.* **100**, 043903 (2008).
- [35] A. Peña, A. Girschik, F. Libisch, S. Rotter, A. A. Chabanov, *Nat. Comm.* **5**, 3488 (2014).
- [36] X. Cheng, X. Ma, M. Yepez, A. Z. Genack, P. A. Mello, *Phys. Rev. B* **96**, 180203(R) (2017)
- [37] C. Kittel, *Introduction to Solid State Physics*, 8th Ed. (John Wiley & Sons, N.J. 2005).
- [38] F. M. Izrailev, A. A. Krokhin, and N. M. Makarov, *Phys. Rep.* **512** (2012) 125.
- [39] H. L. Calvo and H. M. Pastawski, *EPL*, **89** (2010) 60002.
- [40] J. A. Franco-Villafañe, E. Sadurní, S. Barkhofen, U. Kuhl, F. Mortessagne, and T. H. Seligman, *Phys. Rev. Lett.* **111**, 170405 (2013).
- [41] C. Poli, M. Bellec, U. Kuhl, F. Mortessagne, H. Schomerus, *Nat. Commun.* **6**, 6710 (2015)
- [42] Z. L. Mádi, B. Brutscher, T. Schulte-Herbrüggen, R. Brüschweiler, and R. R. Ernst, *Chem. Phys. Lett.* **268**, 300 (1997).
- [43] H. M. Pastawski, G. Usaj, and P. Lewenstein, *Chem. Phys. Lett.* **261**, 329 (1996).
- [44] H. Schanze, H. -J. Stöckmann, M. Martinez-Mares, C. H. Lewenkopf, *Phys. Rev. E* **71**, 016223 (2005).
- [45] T. Dittrich, B. Mehlig, H. Schanz, and U. Smilansky, *Chaos Solitons & Fractals*, **8**, 1205 (1997).
- [46] G. A. Luna-Acosta, J. A. Mendez-Bermudez, and F. M. Izrailev, *Phys. Rev. E*, **64**, 036206 (2001).
- [47] C. Dembowski, H.-D. Gräf, R. Hofferbert, H. Rehfeld, A. Richter, and T. Weiland, *Phys. Rev. E* **60** 3942 (1999).
- [48] B. Gérardin, J. Laurent, A. Derode, C. Prada and A. Aubry, *Phys. Rev. Lett.* **113** 173901 (2014).
- [49] G. E. Mitchell, A. Richter, and H. A. Weidenmüller, *Rev. Mod. Phys.* **82** 2845 (2010).
- [50] D. Page, J. M. Lattimer, M. Prakash, A. W. Steiner, “Stellar Superfluids” in “Novel Superfluids, Volume 2”, edited by K. H. Bennemann and J. B. Ketterson (Oxford University Press, 2014); See also A. Gezerlis, C. J. Pethick, and A. Schwenk, “Pairing and superfluidity of nucleons in neutron stars”, *ibid*.
- [51] T. Takatsuka and R. Tamagaki, *Prog. Theor. Phys.*, **62**, 1655 (1979).